6th European Conference on Computational Mechanics (ECCM 6)
7th European Conference on Computational Fluid Dynamics (ECFD 7)
11âĂŞ15 June 2018, Glasgow, UK

FAILURE ANALYSIS OF ADHESIVE BONDS WITH POLYMORPHIC UNCERTAINTIES: EXPERIMENT AND SIMULATION

MARTIN DRIESCHNER[1], YURI PETRYNA[1], ROBERT GRUHLKE[2], MARTIN EIGEL[2] AND DIETMAR HÖMBERG[2]

[1] Department of Civil Engineering, Technische Universität Berlin
Gustav-Meyer-Allee 25, 13355 Berlin, Germany
martin.drieschner@tu-berlin.de, yuriy.petryna@tu-berlin.de, www.statik.tu-berlin.de

[2] Weierstraß-Institut für Angewandte Analysis und Stochastik (WIAS) Berlin
Mohrenstraße 39, 10117 Berlin, Germany
robert.gruhlke@wias-berlin.de, martin.eigel@wias-berlin.de, dietmar.hoemberg@wias-berlin.de,
www.wias-berlin.de

Key words: Aleatoric and epistemic uncertainty, Fuzzy-stochastic finite element approach, Structural failure quantification

Abstract. This study has been performed within the research project MuScaBlaDes: "Multi-scale failure analysis with polymorphic uncertainties for optimal design of rotor blades", which is part of the DFG Priority Program (SPP 1886) "Polymorphic uncertainty modelling for the numerical design of structures" started in 2016. One of the typical failure mechanisms of rotor blades in operation are fatigue cracks in adhesive bonds that are in the focus of our project. Depending on the manufacturing process, the failure is often caused by air voids whose properties could be generally quantified by non-destructive testing (NDT) on a representative sub-component, called the Henkel beam. By using the NDT data, we simulate structural failure by means of a fuzzy-stochastic finite element approach and compare numerical simulations with real experiments on representative specimens to validate the uncertainty models. For solving polymorphic problems a MATLAB® framework called PolyUQ has been developed and the current state of this ongoing work will be presented and discussed at the conference.

1 INTRODUCTION

Rotor blades of wind turbines are thin-walled spatial structures typically consisting of two composite shells and one or two shear webs. The structural components are assembled with adhesive bonds whose quality affects the overall integrity and reliability of rotor blades. Within the research project MuScaBlaDes: "Multi-scale failure analysis with polymorphic uncertainties for optimal design of rotor blades", see Fig. 1, we focus on the failure caused by debonding which has been identified as a reason for structural collapse in a full-scale rotor blade test [1].

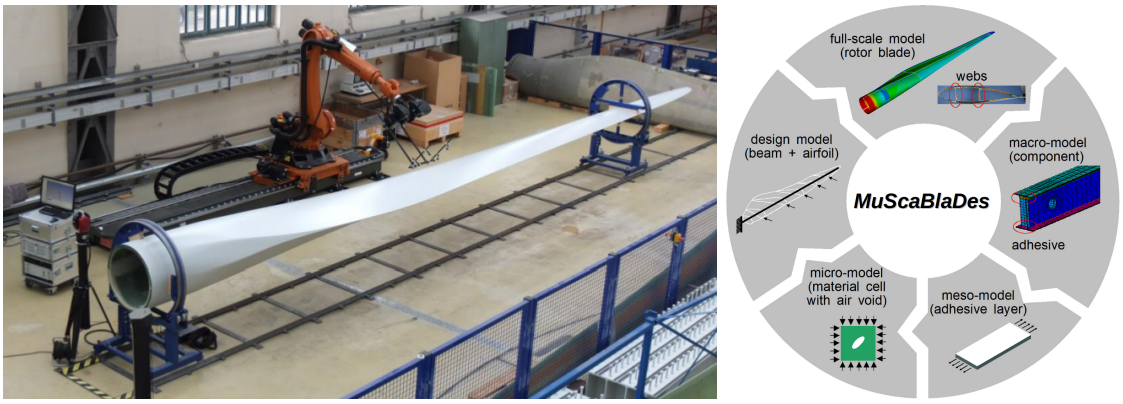

Figure 1: Rotor blade at TU Berlin as focus in research project MuScaBlaDes

In this regard, representative sub-components, e.g. the Henkel beam by the Fraunhofer Institute for Wind Energy and Energy System Technology [2], have been developed in the past for experimental investigations. It could be seen that the fatigue damage mechanism is initiated by multiple cracks in the adhesive bonds due to air voids and debonding. For understanding the reasons of failure, various non-destructive testing (NDT) has been applied by TU Berlin within the BladeTester project [3]. The obvious assumption that the crack initiation is probably caused by a critical stress concentration around the air void inclusions is analysed in this study by means of a finite element approach in consideration of polymorphic uncertainties. Epistemic uncertainties originate here from the NDT data, limited information and subjectivity, whereas aleatoric uncertainties result from natural variability of uncertain variables on the other hand. As an extension of a pure stochastic approach [4] the resulting polymorphic output displays the influences of different uncertainty sources to the relative bearing capacity of adhesive bonds. Defuzzified stochastic values like mean value or selected fractile values can finally be used for the assessment of air voids in a structural failure analysis.

To validate the numerical models with polymorphic uncertainties, we investigate the structural failure in real experiments of representative specimens. Polymorphic uncertainties have been taken into account in a realistic manner, e.g. from standardised testing and experimental inaccuracies. The simulation results are then compared to the experimentally determined failure mechanisms as well as ultimate loads.

2 NON-DESTRUCTIVE TESTING OF ADHESIVE BONDS

Within the BladeTester project [3], ten Henkel beams (Fig. 2) have been used for various studies of adhesive bonds. Both artificial voids of relatively large sizes and natural voids due to various mixing procedures and material properties have been investigated. For three Henkel beams (HB) with artificial and natural air voids - namely HB3, HB9 and HB10 - usual computer tomography (CT) devices have been applied, see [5] for more information. The CT results are at disposal with a resolution of 3mm and partly with a resolution of 0.8mm in longitudinal direction.

Using the Image Processing Toolbox in MATLAB®, the analysis of the air void prop-

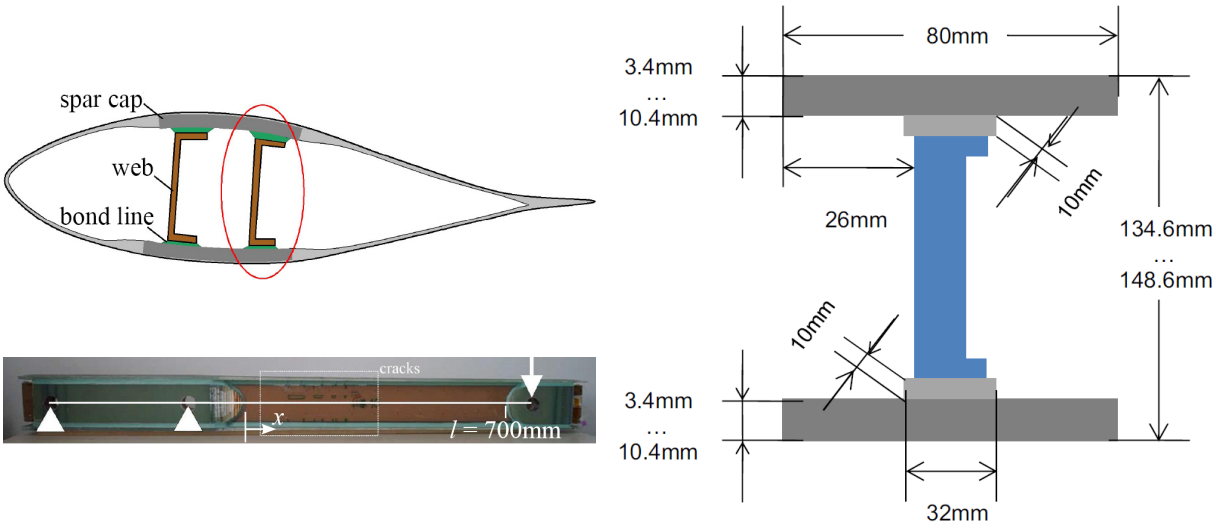

Figure 2: Henkel beam geometry and relation to rotor blade according to [2]

erties is done with the following procedure:

1. detection of the region of interest with a length of $l = 700\text{mm}$, see Fig. 2
2. for all relevant two-dimensional CT images
   (a) import of the RGB image
   (b) converting in a gray image
   (c) detection of the two adhesive bonds in the Henkel beam
   (d) for all adhesive bonds
      i. image binarization
      ii. analysis of the air void properties, e.g. amount, position and size
      iii. calculation of the air voids content ϕ
3. visualization in a x-ϕ-diagram, see Fig. 3.

For the numerical simulations of adhesive bonds, it is useful to simplify the calculated air voids content ϕ. The red line in Fig. 3 describes the numerical approximation and an exemplary adhesive bond structure is shown below the diagram. To mention is that all air voids with a content less than 5% in the two-dimensional CT image are neglected in this study. Furthermore, the converting of the RGB values to a scalar gray value, the gray image analysis and the image binarization require settings which obviously influence the calculated air void properties. Six adhesive bonds have been taken into account in total and the corresponding numerical simulations will be described in Section 3.

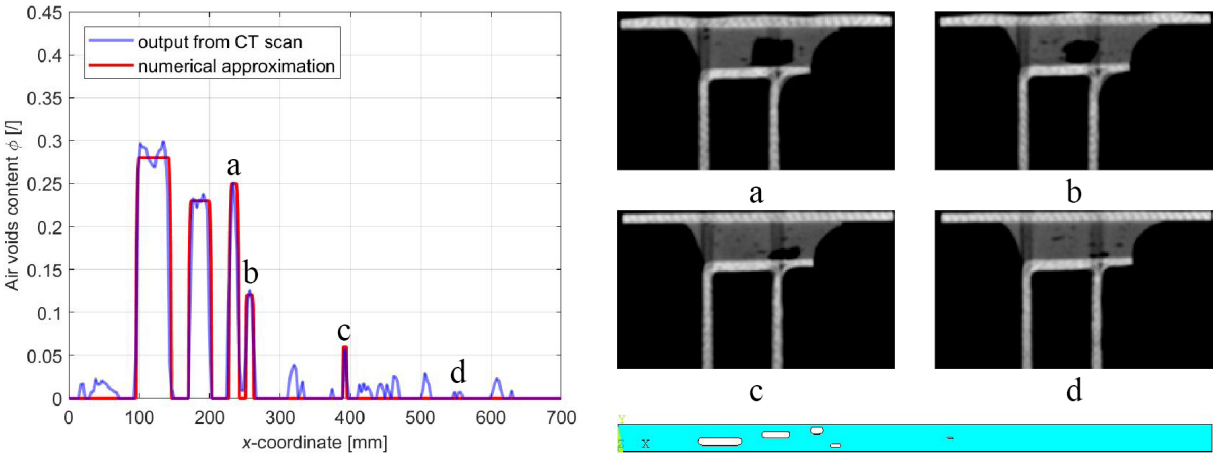

Figure 3: Air voids content of Henkel beam 10 - adhesive bond 1 with associated numerical model

3 NUMERICAL SIMULATIONS OF ADHESIVE BONDS

3.1 Numerical model for adhesive bonds

For the development of a numerical model, we focus on static loading of the Henkel beam. Due to elastic behaviour and present geometrical dimensions, the beam theory is valid which leads to a linear strain and stress distribution over the beam height. Furthermore, the stress distribution over the adhesive bonds can be considered as constant caused by the relatively small adhesive bond thickness compared to the Henkel beam height. To avoid time-consuming numerical simulations, the adhesive bond is defined as a two-dimensional plate with length $l = 700$mm in x-direction and width $b = 32$mm in y-direction with constant thickness $t = 10$mm under plane stress. The plate is made of epoxy resin. We assume a linear elastic material behaviour until the first cracking that means local failure. It corresponds to a brittle behaviour which is typical under fatigue loading of adhesive bonds. The plate is fixed at one edge ($x = 0$mm) and uniformly loaded in x-direction at another edge ($x = 700$mm). The relative bearing capacity $F_{\max}/F_{\text{ideal}}$ as ratio of the ultimate tensile load with air voids to the ultimate tensile load without air voids is defined as quantity of interest and depends on the air void configuration inside the adhesive bond.

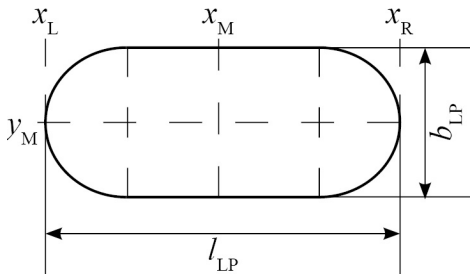

Figure 4: Air void simplified as slotted hole

It could be seen in Section 2 that air voids exhibit various dimensions and shapes. According to the air void content ϕ_{LP}, each air void is simplified as slotted hole and can be described with the following five parameters, see also Fig. 4:

- midpoint location x_{M}
- midpoint location y_{M}
- width b_{LP} which is calculated by $b_{\mathrm{LP}} = \phi_{\mathrm{LP}} b$
- length l_{LP} which is calculated by $l_{\mathrm{LP}} = v_{\mathrm{LP}} b_{\mathrm{LP}}$ with an air void size ratio v_{LP}
- rotation in x-y-plane α_{LP} which is set to $\alpha_{\mathrm{LP}} = 0°$ for simplification

3.2 Consideration of polymorphic uncertainties

Limited information on the amount and size of air voids as well as subjective settings in the CT image analysis lead to epistemic uncertainties whereas natural variability and randomness of the air void location lead to aleatoric uncertainties. Both types together require a structural failure analysis with polymorphic uncertainties, which are listed in Table 1. The total number of uncertain input variables depends on the number of air

Table 1: Input variables for adhesive bond simulations

name	unit	type	values
plate length	[mm]	deterministic	$l =$ 700
plate width	[mm]	deterministic	$b =$ 32
plate thickness	[mm]	deterministic	$t =$ 10
Young's modulus	[MPa]	deterministic	$E =$ 4890
Poisson's ratio	[/]	deterministic	$\nu =$ 0.22
uniaxial loading	[N]	deterministic	$F =$ 1
numerical parameter	[mm]	deterministic	$\epsilon =$ 0.5
number of air voids	[/]	fuzzy	$n_{\mathrm{LP}} =$ TFI $\langle 0; 2; 4; 6 \rangle$
ith air voids content	[/]	interval	$\phi_{\mathrm{LP}i} \in$ $[0.05; 0.40]$
ith air voids size ratio	[/]	interval	$v_{\mathrm{LP}i} \in$ $[1.00; 7.00]$
midpoint x-location of air void i	[mm]	stochastic	$x_{\mathrm{M}i} \sim \mathcal{U}(a_{\mathrm{x}i}; b_{\mathrm{x}i})$
midpoint y-location of air void i	[mm]	stochastic	$y_{\mathrm{M}i} \sim \mathcal{U}(a_{\mathrm{y}i}; b_{\mathrm{y}i})$

voids n_{LP} itself an uncertain parameter. The air voids content ϕ_{LP} and the air voids size ratio $v_{\mathrm{LP}} = l_{\mathrm{LP}}/b_{\mathrm{LP}}$ have been defined based on the CT image analysis in Section 2.

The bounds of the uniform distribution for the midpoint location x_{M} are calculated for each air void $i = \{1, \ldots, n_{\mathrm{LP}}\}$ as follows: An effective length $l_{\mathrm{eff}} = l - 2b$ is divided in equidistant subdomains with a length of $l_i = l_{\mathrm{eff}}/n_{\mathrm{LP}}$ and bounds $[x_{\mathrm{min},i}; x_{\mathrm{max},i}] = [b + (i-1)l_i; b + il_i]$ in x-direction. To avoid numerical problems, the equation $x_{\mathrm{min},i} + \epsilon \leq x_{\mathrm{L}i} < x_{\mathrm{R}i} \leq x_{\mathrm{max},i} - \epsilon$ has to be valid for each slotted hole. The relation $x_{\mathrm{M}i} =$

$(x_{\mathrm{L}i} + x_{\mathrm{R}i})/2$ leads to

$$a_{\mathrm{x}i} = x_{\min,i} + \epsilon + \frac{l_{\mathrm{LP}i}}{2} = b + (i-1)\frac{l-2b}{n_{\mathrm{LP}}} + \epsilon + \frac{v_{\mathrm{LP}i}\phi_{\mathrm{LP}i}b}{2} \tag{1}$$
$$b_{\mathrm{x}i} = x_{\max,i} - \epsilon - \frac{l_{\mathrm{LP}i}}{2} = b + i\frac{l-2b}{n_{\mathrm{LP}}} - \epsilon - \frac{v_{\mathrm{LP}i}\phi_{\mathrm{LP}i}b}{2}.$$

With the condition that each air void is completely located inside the plate one obtains

$$a_{\mathrm{y}i} = \frac{b_{\mathrm{LP}i}}{2} = \frac{\phi_{\mathrm{LP}i}b}{2} \tag{2}$$
$$b_{\mathrm{y}i} = b - \frac{b_{\mathrm{LP}i}}{2} = b - \frac{\phi_{\mathrm{LP}i}b}{2}$$

for the bounds of the uniform distribution for the midpoint location y_{M}.

3.3 Solving and results

A MATLAB® framework called PolyUQ has been developed inhouse for solving polymorphic problems also with an integrated interface to black-box solvers, see Fig. 5.

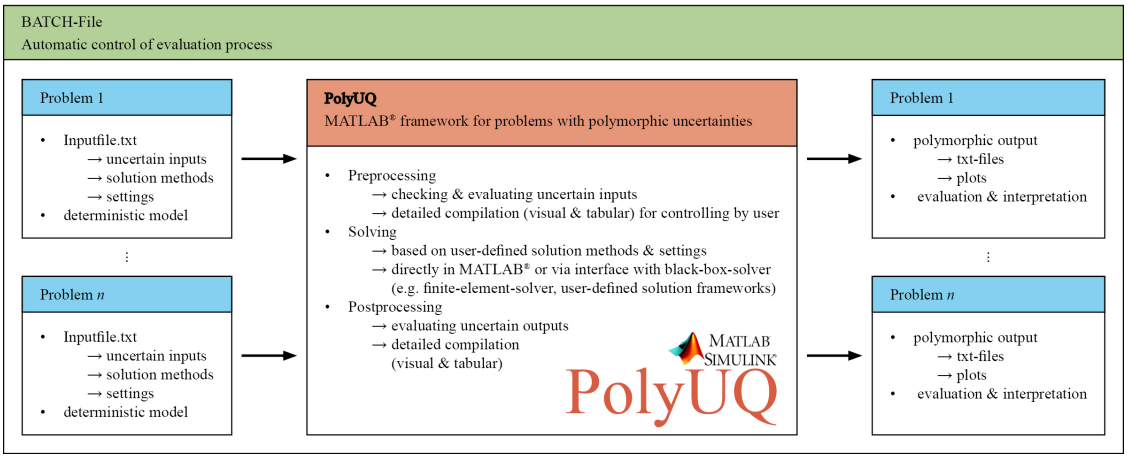

Figure 5: MATLAB® framework PolyUQ

The described numerical model and the input variables have already been defined above. In addition

- the reduced transformation method for the fuzzy variable [6],
- the vertex method for the interval variables [7] and
- the Monte Carlo Sampling as well as the Latin Hypercube Sampling with $n = 10^3$ simulations at maximum in each fuzzy-interval configuration for the stochastic variables [8]

have been selected as solution methods. Fig. 6 displays the fuzzy-interval-stochastic and defuzzified output for the relative bearing capacity $F_{\max}/F_{\text{ideal}}$. For defuzzification, many methods are discussed in the literature (e.g. in [9]) and the centroid method was chosen for the worst case. For the discrete worst case membership function in blue with $(x_i; \mu(x_i))$ the centroid values c in green are calculated as

$$c = \frac{\sum x_i \mu(x_i)}{\sum \mu(x_i)}. \tag{3}$$

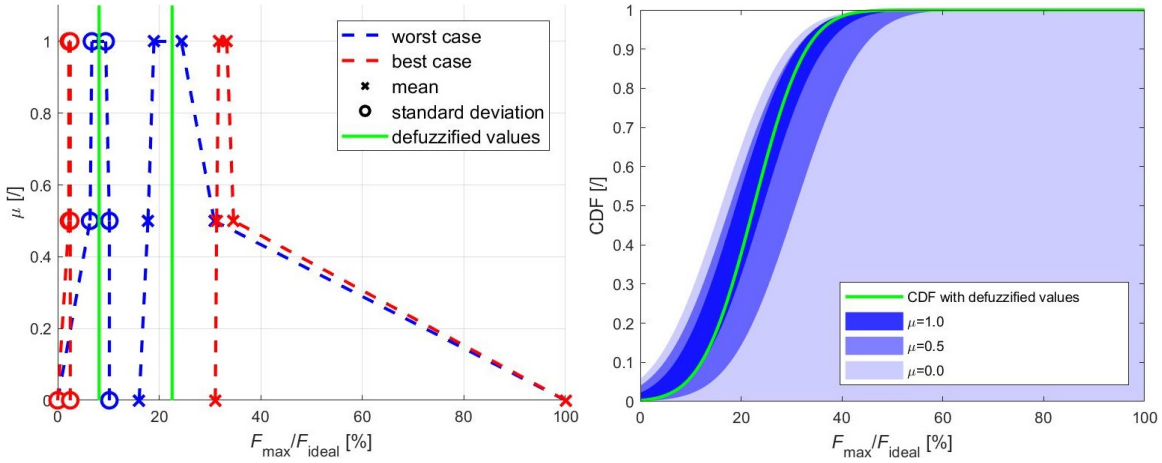

Figure 6: Fuzzy-interval-stochastic output and corresponding defuzzification

Finally, Fig. 7 shows the convergence of the defuzzified mean to a value of 22% and of the standard deviation to a value of 8% respectively with increasing number of simulations.

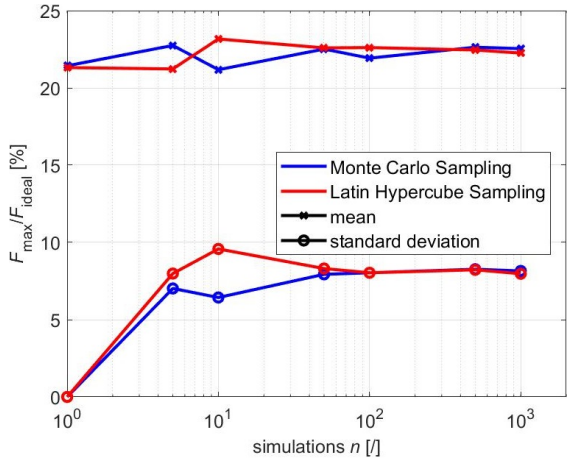

Figure 7: Convergence plot of defuzzified stochastic values

4 REAL EXPERIMENTS ON REPRESENTATIVE SPECIMENS

For the validation of our numerical models with polymorphic uncertainties, we investigate the structural failure of a plate under uniaxial tensile loading and compare the experimental results with the numerical solutions. As a representative material for epoxy resin described in Section 3.1 we have chosen an acryl glass - Plexiglas® XT transparent - where we expect a similar failure mechanism. At that, the holes in the plate shall affect the failure mechanism in a similar way as the air voids in the adhesive bond. Fig. 8 displays the experimental setup and the specimens after testing with the associated ultimate load $F_{\max}$ and crack pattern that we call failure mechanism (FM).

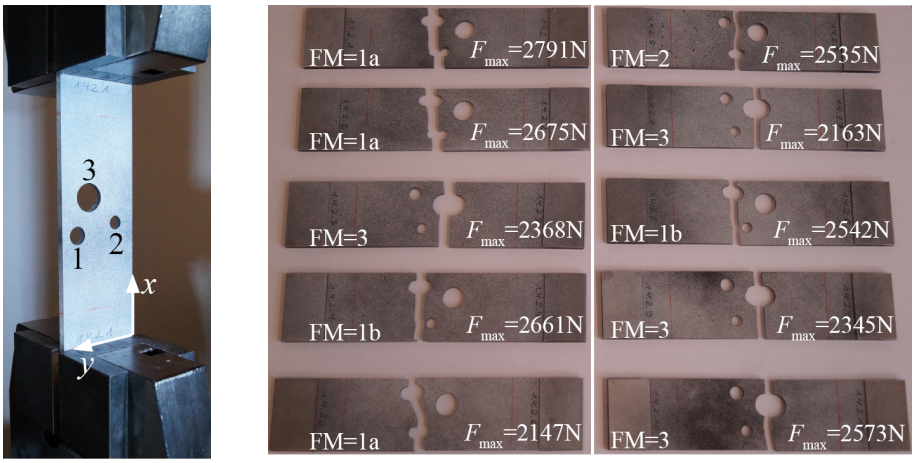

Figure 8: Uniaxial testing at TU Berlin

Based on uncertain material properties, determined through standardised testing according to [10], geometrical imperfections and experimental inaccuracies, we have defined diverse uncertain variables, see Table 2. Compared to Section 3, the number of holes is deterministic and the holes are circular so that the size will be defined through the diameter as an interval variable. The x- and y-location of each hole are uniformly distributed variables with a small scatter, respectively.

As can be seen from Fig. 8, the plate exhibits a scatter of ultimate load and various crack patterns, i.e. quantitative and qualitative differences of failure mechanism. In the numerical simulations different first crack locations can also be detected through uncertain input variables which naturally leads to different failure mechanisms. The first crack location is equivalent to the location of the maximum stress concentration caused by uniaxial tensile loading, see Fig. 9.

Analogously to the experiments, the lower edge is fixed and the upper edge is loaded. The structural failure is reached if the maximum first principal stress in the structure exceeds the tensile strength, so that $\max(\sigma_1) = f_{\mathrm{t}} = 64\mathrm{MPa}$. Fig. 10 shows the numerical results and illustrates that all ten experimental ultimate loads could be find within a 90% confidence interval. The lowest experimental value $F_{\max} = 2147\mathrm{N}$ corresponds to an interval fractile value of $[5\%; 12\%]$ and the highest experimental value $F_{\max} = 2791\mathrm{N}$

Table 2: Input variables for Plexiglas® simulations

name	unit	type	values
plate length	[mm]	deterministic	$l =$ 150
plate width	[mm]	deterministic	$b =$ 50
plate thickness	[mm]	deterministic	$t =$ 4
Poisson's ratio	[/]	deterministic	$\nu =$ 0.38
number of holes	[/]	deterministic	$n =$ 3
tensile strength	[MPa]	deterministic	$f_\mathrm{t} =$ 64
Young's modulus	[MPa]	stochastic	$E \sim \mathcal{N}(3230; 469)$
load angle	[°]	stochastic	$\alpha \sim \mathcal{U}(-2; +2)$
hole 1 x-location	[mm]	stochastic	$x_1 \sim \mathcal{U}(61; 65)$
hole 1 y-location	[mm]	stochastic	$y_1 \sim \mathcal{U}(38; 42)$
hole 2 x-location	[mm]	stochastic	$x_2 \sim \mathcal{U}(67; 71)$
hole 2 y-location	[mm]	stochastic	$y_2 \sim \mathcal{U}(11; 15)$
hole 3 x-location	[mm]	stochastic	$x_3 \sim \mathcal{U}(82; 86)$
hole 3 y-location	[mm]	stochastic	$y_3 \sim \mathcal{U}(30; 34)$
hole 1 diameter	[mm]	interval	$d_1 \in [9.5; 10.5]$
hole 2 diameter	[mm]	interval	$d_2 \in [7.5; 8.5]$
hole 3 diameter	[mm]	interval	$d_3 \in [15.5; 16.5]$

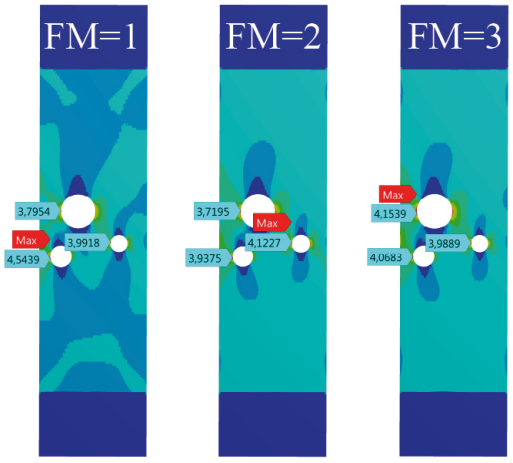

Figure 9: Different first crack locations caused by uncertainties

corresponds to an interval fractile value of $[43\%; 71\%]$, respectively.

The vertex method [7] is used for the interval space whereby the methods

- Monte Carlo Sampling with maximal $n = 10^4$ simulations,
- Latin Hypercube Sampling with maximal $n = 10^4/2$ simulations and
- Sparse Grid with Clenshaw-Curtis Nodes and a maximal sparse grid level of $l = 4$

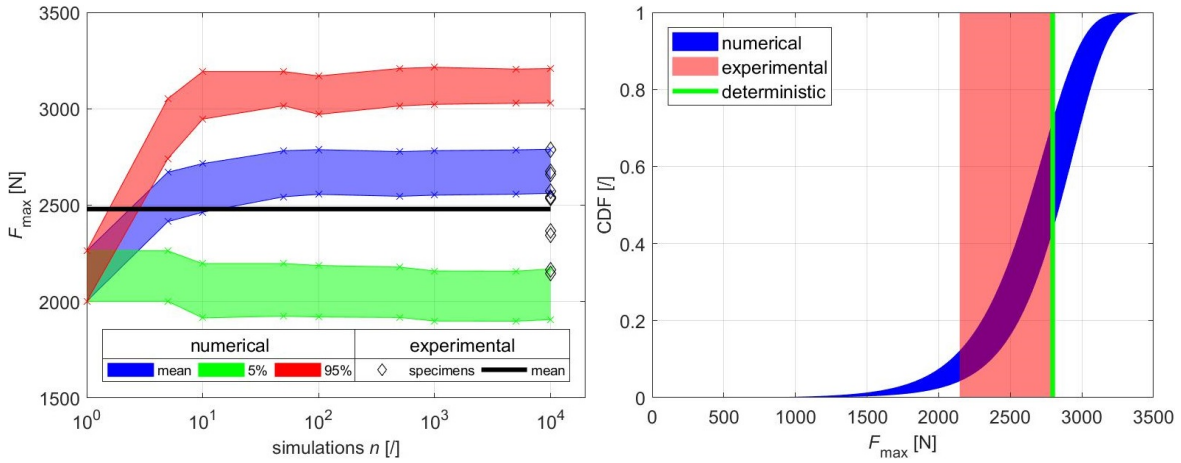

Figure 10: Interval stochastic output

are compared for the stochastic space [8]. Fig. 11 displays a fast convergence of the interval mean and the interval standard deviation with increasing number of simulations independently from the chosen method.

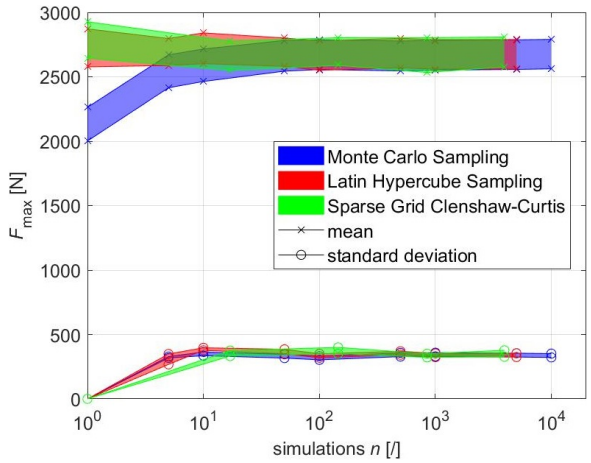

Figure 11: Convergence plot of interval stochastic values

5 CONCLUSIONS

In the present study, the structural failure of adhesive bonds in the presence of polymorphic uncertainties is investigated numerically as well as experimentally on representative specimens.

The proposed numerical model is based on experimental data obtained by computer tomography of a representative sub-component. Natural variability, imprecise scanning and limited information lead to aleatoric and epistemic uncertainties which are taken into account in a fuzzy-interval-stochastic finite element approach. Adhesive bonds with air voids have shown a considerably smaller bearing capacity in comparison with an adhesive

bond free of air voids.

Furthermore, real experiments of an acryl glass - Plexiglas® XT transparent - have been executed at TU Berlin for validation of the numerical models. Ten specimens consisting of three holes have been loaded by uniaxial tension and various experimental failure mechanisms could also be reproduced in the numerical solutions. The numerical model has been defined in a polymorphic sense and finally yields a 90% confidence interval of [1907N; 3031N] at worst in which all experimentally determined ultimate loads could be covered. Like in the previous analysis of adhesive bonds, different numerical methods have been compared and have shown similar convergence rates.

6 ACKNOWLEDGEMENT

The authors gratefully acknowledge financial support of the German Research Foundation (DFG) within the Research Project MuScaBlaDes.

REFERENCES

[1] Yang, J., Peng, C., Xiao, J., Zeng, J., Xing, S., Jin, J. and Deng, H. Structural investigation of composite wind turbine blade considering structural collapse in full-scale static tests. *Composite Structures* (2013) **97**:15–29.

[2] Sayer, F., Antoniou, A. and van Wingerde, A. Investigation of structural bond lines in wind turbine blades by sub-component tests. *International Journal of Adhesion & Adhesives* (2012) **37**:129–135.

[3] Petryna, Y. *Collaborative Research Project BladeTester - Final Report*. DOI: 10.2314/GBV:848718607, 2015.

[4] Kovačević, D., Petryna, Y. and Petronijević, M. *Assessment of the impact of air voids on adhesive joints in rotor blades by use of NDT and FEA*. EWSHM, 2016.

[5] Künzel, A. *Parameteridentifikation auf Basis faseroptisch gemessener quasi-kontinuierlicher Dehnungssignale*. TU Berlin, 2016.

[6] Hanss, M. *Applied Fuzzy Arithmetic - An Introduction with Engineering Applications*. Springer, 2005.

[7] Dong, W. and Shah, H. Vertex Method for Computing Functions of Fuzzy Variables. *Fuzzy Sets and Systems* (1987) **24**:65–78.

[8] Xiu, D. *Numerical Methods for Stochastic Computation*. Princeton University Press, 2010.

[9] Möller, B. and Beer, M. *Fuzzy Randomness - Uncertainty in Civil Engineering and Computational Mechanics*. Springer, 2004.

[10] DIN Deutsches Institut für Normung e. V., *EN ISO 527: Kunststoffe - Bestimmung der Zugeigenschaften*. Beuth, 2012.